Theory and simulation of the interaction of ultraintense laser pulses with electrons in vacuum

Brice Quesnel and Patrick Mora
Centre de Physique Théorique (UMR 7644 du CNRS), Ecole Polytechnique, 91128 Palaiseau Cedex, France
(Received 15 January 1998)

In order to investigate ponderomotive force in the relativistic regime, the interaction of ultraintense laser pulses with free electrons in vacuum is studied both theoretically and numerically. Various expressions for the electromagnetic field of the laser in the case of a Gaussian transverse profile are given, which take into account corrections to the monochromatic paraxial approximation, and the effects of finite pulse duration. A detailed demonstration of relativistic ponderomotive force (RPF) is established which makes apparent the domain of validity of this concept. Computer simulations are carried out using a three-dimensional test-particle code. They show the importance of the correct description of the fields, and confirm the domain of validity of the RPF which is $1-v_z/c \gg 1/kw_0$, where v_z is the component of the electron velocity parallel to the laser propagation direction, c is the velocity of light, k is the laser wave vector, and w_0 the beam waist at focus. Outside of this domain, the electron motion is more complicated, with a high sensitivity on the initial distance from the laser propagation axis and a relatively low energy gain. [S1063-651X(98)02409-X]

PACS number(s): 52.65.Cc, 42.50.Vk, 41.20.−q, 52.60.+h

I. INTRODUCTION

With the development of ultraintense lasers [1], it is now usual to create electromagnetic fields where the quiver velocity of an electron approaches c at focus. In these conditions, the question has arisen of the validity of the concept of ponderomotive force. At low laser intensities, it is well known [2,3] that the averaged motion of an electron in the focus of a laser can be described as a slow drift toward the regions of low field intensity. The corresponding averaged equation of motion for the electron is written

$$\frac{d\overline{\mathbf{p}}}{dt} = -\frac{e^2}{2m\omega^2}\nabla\overline{|\mathbf{E}|^2}, \tag{1}$$

where $\mathbf{p}$ is the electron momentum, e the elementary charge, m the electron mass, ω the laser frequency, and $\mathbf{E}$ the electric field of the laser wave, and where the overbar denotes an average over the laser period. This nonrelativistic regime corresponds to the case $a \ll 1$, where $a = eE/mc\omega$ is the normalized amplitude of the electromagnetic field of the laser.

In the relativistic regime ($a \geqslant 1$), various studies have been reported. On the one hand, a new definition of the ponderomotive potential has been given [4–8] through a fully relativistic calculation. It concludes that the main features of the nonrelativistic case still apply: the averaged electron motion is independent of the laser polarization, and the electrons are expelled from the high-intensity regions. This relativistic ponderomotive force (RPF) is a valid description provided that the wave amplitude varies slowly with respect to the wave phase, so that a multiple scale analysis of the particle motion can be performed. On the other hand, two-dimensional (2D) computer simulations have been made in the relativistic regime for a linearly polarized wave, which conclude that at very high intensity the laser-electron interaction is terminated within a wavelength, and the electron is scattered away from focus with a very high escape energy [9]. This so called high-intensity ponderomotive scattering is expected to occur when the electron quiver amplitude reaches the beam waist at focus. References [10–12] recently reported an experiment designed on the basis of this second description, which also concluded that the electron is expelled from the focus in the plane of polarization of the wave.

It must be noted, however, that as this effect is most important in regions of high field gradient, i.e., at focus, some care has to be taken in the description of the electromagnetic field. It is well known indeed that the usual scalar description of the field as a Gaussian mode [13] used in Refs. [9] and [10] is only a lowest order approximation for the fields. Longitudinal components of the field appear at the next order [14–17] which play an important role in the correct description of the classical ponderomotive force [18].

This paper is aimed at clarifying the discrepancy between these two relativistic generalizations of the ponderomotive motion. As the paraxial approximation is known to be insufficient, we first derive the exact expressions of all the components of the electromagnetic field around the focus for the usual case of a Gaussian transverse profile. These components are correct to all orders with respect to the paraxial approximation. For very short pulses, other corrections due to the fact that the light is no longer strictly monochromatic have to be taken into account. We also derive the first order correction arising from this effect. We then derive the RPF [6,7] in the special case of propagation in vacuum, insisting on the theoretical conditions of validity of this calculation. We compare our result with similar ones found in the literature [4,5,8]. We present a 3D test-particle simulation program designed to check the validity of this concept numerically. We use this code to study the same case as Hartemann *et al.* [9], and show that their 2D model is clearly insufficient. Similarly, we demonstrate the incompleteness of the simulations supporting the experiment of Ref. [10] and the validity of the RPF in this regime of parameters [11]. We conclude with the necessity of additional experiments.

II. ELECTROMAGNETIC FIELD NEAR FOCUS

Here we are interested in a correct description of the focalized electromagnetic field of a laser. We will recall various works that have already been done on the subject, show how they can be unified to give a coherent and complete description of the electromagnetic field around focus in vacuum for a Gaussian laser profile, and derive a convenient way to take into account the effects due to the short duration of the pulse. In the rest of this paper, the laser field propagates in the z direction.

A. Angular spectrum representation of plane waves

The angular spectrum representation of plane waves is a powerful method to obtain an exact expression for the fields of a focalized laser wave [16,18–22]. In this formalism, two transverse components of the field have to be given in the focal plane, and then all components can be deduced at any point in space. We will first consider a monochromatic (and thus infinitely long) pulse, with frequency ω_0. For convenience, in the expression of the fields we suppress the $e^{-i\omega_0 t}$ time dependence. We take as a starting component the transverse electric field, which we suppose to be polarized in the x direction and with a Gaussian profile with beam waist at focus w_0, $E_x(x,y,z=0)=E_0\exp[-(x^2+y^2)/w_0^2]$. We can write its transverse Fourier transform as

$$\tilde{E}_x(p,q)=\frac{1}{\lambda_0^2}\int\int E_x(x,y,0)e^{-ik_0(px+qy)}dx\ dy$$

$$=\frac{E_0}{4\pi\epsilon^2}\exp[-(p^2+q^2)/4\epsilon^2], \tag{2}$$

where $\lambda_0=2\pi c/\omega_0$ is the laser wavelength in vacuum, $k_0=\omega_0/c$ is the corresponding wave vector, and $\epsilon=1/k_0w_0$ is a small quantity. It is then easy to show that E_x can be computed at any point in space using

$$E_x(x,y,z)=\int\int \tilde{E}_x(p,q)\exp[ik_0(px+qy+mz)]dp\ dq, \tag{3}$$

where

$$m=\begin{cases}(1-p^2-q^2)^{1/2} & \text{if } p^2+q^2\leqslant 1\\ i(p^2+q^2-1)^{1/2} & \text{if } p^2+q^2>1.\end{cases} \tag{4}$$

E_y is usually taken as a second known component [14,18], with $E_y=0$ at focus, so that $E_y=0$ exactly and everywhere in space. The other components of the fields can then be calculated using the Maxwell equations. For instance E_z is given by $\boldsymbol{\nabla}\cdot\mathbf{E}=0$, so that

$$E_z(x,y,z)=\frac{i}{k_0}\frac{\partial}{\partial x}\int\int \tilde{E}_x(p,q)\frac{\exp[ik_0(px+qy+mz)]}{m}dp\ dq. \tag{5}$$

However [17], the fields lack symmetry in that $E_y=0$ but $B_x\neq 0$. To obtain a physically more reasonable symmetric expression of the fields, we only need to repeat the same analysis, starting from B_y instead of E_x. We take for $B_y(z=0)$ the same Gaussian profile as for $E_x(z=0)$, and we suppose that $B_x=0$. We then deduce all fields everywhere in space. The final expression of the fields is simply half the sum of the two results. All six components are then different from zero. In order to simplify some demonstrations in this section, we will work in some cases with the (simplest) nonsymmetrized expression of the fields that we will distinguish from the symmetrized ones with a hat: $\hat{E}_x$ is the nonsymmetrized value of the E_x field.

To continue the derivation, we notice that the value of m in Eq. (4) when $p^2+q^2>1$ gives evanescent waves which can be neglected to a very good approximation as a consequence of Eq. (2) and of the small values of ϵ considered throughout this paper (typically, $\epsilon<3.2\times10^{-2}$). Thus, the integral in Eq. (3) is restricted to $p^2+q^2<1$. The remaining part of the integrals is calculated in cylindrical coordinates, which gives for the case of $\hat{E}_x$:

$$\hat{E}_x(x,y,z)=\frac{E_0}{2\epsilon^2}\int_0^1 e^{-b^2/4\epsilon^2}e^{ik_0z\sqrt{1-b^2}}J_0(k_0rb)b\ db, \tag{6}$$

where $b=\sqrt{p^2+q^2}$ and $r=\sqrt{x^2+y^2}$. If we eventually reintroduce the temporal dependence and the terms coming from B_y, and if we take the real part of the expressions, we obtain the following equations for the fields:

$$E_x=\frac{E_0}{4\epsilon^2}\left(I_1+\frac{x^2-y^2}{k_0r^3}I_2+\frac{y^2}{r^2}I_3\right), \tag{7a}$$

$$E_y=-\frac{E_0}{4\epsilon^2}\frac{xy}{k_0r^3}(k_0rI_3-2I_2), \tag{7b}$$

$$E_z=\frac{E_0}{4\epsilon^2}\frac{x}{r}I_4, \tag{7c}$$

$$B_x=\frac{E_y}{c}, \tag{7d}$$

$$B_y=\frac{E_0}{4c\epsilon^2}\left(I_1+\frac{y^2-x^2}{k_0r^3}I_2+\frac{x^2}{r^2}I_3\right), \tag{7e}$$

$$B_z=\frac{E_0}{4c\epsilon^2}\frac{y}{r}I_4, \tag{7f}$$

where

$$I_1=\int_0^1 e^{-b^2/4\epsilon^2}(1+\sqrt{1-b^2})\sin(\phi_b)J_0(k_0rb)b\ db, \tag{8a}$$

$$I_2=\int_0^1 e^{-b^2/4\epsilon^2}\frac{\sin(\phi_b)}{\sqrt{1-b^2}}J_1(k_0rb)b^2db, \tag{8b}$$

$$I_3=\int_0^1 e^{-b^2/4\epsilon^2}\frac{\sin(\phi_b)}{\sqrt{1-b^2}}J_0(k_0rb)b^3db, \tag{8c}$$

$$I_4=\int_0^1 e^{-b^2/4\epsilon^2}\left(1+\frac{1}{\sqrt{1-b^2}}\right)\cos(\phi_b)J_1(k_0rb)b^2db, \tag{8d}$$

and where $\phi_b=\omega_0 t-k_0z\sqrt{1-b^2}+\phi_0$, with ϕ_0 an arbitrary constant.

These are exact expressions for the fields in the case of a monochromatic pulse, which means that they satisfy the Maxwell equations exactly. As a consequence of this fact, each component in Eqs. (7) is an exact solution to the scalar wave equation in vacuum:

$$\left(\Delta-\frac{1}{c^2}\frac{\partial^2}{\partial t^2}\right)\Psi=0. \tag{9}$$

These components can be taken as a starting point for the expansion of the fields in powers of ϵ, as shown in Refs. [16] and [18]. One then obtains all the coefficients of this expansion. For simplicity, here we will show the derivation for $\hat{E}_x$ (i.e., without considering the terms coming from B_y, which can be calculated exactly in the same way). The method consists in developing the term $e^{ik_0z\sqrt{1-b^2}}$ in Eq. (6) as

$$e^{ik_0z\sqrt{1-b^2}}=\sum_{n=0}^{\infty}\frac{1}{n!}\left(\frac{b^2}{2}\right)^n(k_0z)^{n+1}h_{n-1}^{(1)}(k_0z), \tag{10}$$

where

$$h_n^{(1)}(v)=\frac{e^{iv}}{v}i^{-(n+1)}\sum_{m=0}^{n}(-1)^m\frac{(n+m)!}{(n-m)!}\left(\frac{1}{2iv}\right)^m$$
$$\text{for } n\geqslant 0,\quad h_{-1}^{(1)}(v)=ih_0^{(1)}(v) \tag{11}$$

is the nth-order spherical Bessel function of the third kind. The remaining integrals in b are then calculated by

$$\int_0^1\epsilon^{-2}e^{-b^2/4\epsilon^2}b^{2n+1}J_0(k_0rb)db$$
$$\simeq\int_0^\infty\epsilon^{-2}e^{-b^2/4\epsilon^2}b^{2n+1}J_0(k_0rb)db$$
$$=2^{2n+1}n!\,\epsilon^{2n}e^{-r^2/w_0^2}L_n(r^2/w_0^2), \tag{12}$$

where $L_n(u)$ is the nth-order Laguerre polynomial. After inversion of the two sums, the final expression of $\hat{E}_x$ reads:

$$\hat{E}_x=E_0e^{ik_0z}e^{-r^2/w_0^2}\left[1+\sum_{m=0}^{\infty}\epsilon^{2m}\sum_{n=0}^{\infty}\frac{(2m+n)!}{n!}\left(\frac{-iz}{z_R}\right)^{(n+1)}L_{m+n+1}\left(\frac{r^2}{w_0^2}\right)\right], \tag{13}$$

where $z_R=k_0w_0^2/2$ is the Rayleigh length. The zero order term in this last equation is simply the paraxial solution for the fields, that is the solution to the paraxial wave equation:

$$\left(\Delta_\perp+2ik\frac{\partial}{\partial z}\right)E=0. \tag{14}$$

All fields have similar expressions, with even powers of ϵ for the transverse ones, and odd powers for the longitudinal one:

$$E_x=E_x^{(0)}+\epsilon^2E_x^{(2)}+\cdots, \tag{15a}$$

$$E_y=\epsilon^2E_y^{(2)}+\cdots, \tag{15b}$$

$$E_z=\epsilon E_z^{(1)}+\epsilon^3E_z^{(3)}+\cdots, \tag{15c}$$

$$B_x=\epsilon^2B_x^{(2)}+\cdots, \tag{15d}$$

$$B_y=B_y^{(0)}+\epsilon^2B_y^{(2)}+\cdots, \tag{15e}$$

$$B_z=\epsilon B_z^{(1)}+\epsilon^3B_z^{(3)}+\cdots. \tag{15f}$$

Here we give the expression for the real parts of the fields up to first order, as will be needed in the following:

$$E_x=E_0\frac{w_0}{w}\exp\left(-\frac{r^2}{w^2}\right)\sin(\phi_G), \tag{16a}$$

$$E_z=2E_0\epsilon\frac{xw_0}{w^2}\exp\left(-\frac{r^2}{w^2}\right)\cos(\phi_G^{(1)}), \tag{16b}$$

$$B_y=\frac{E_x}{c}, \tag{16c}$$

$$B_z=2E_0\epsilon\frac{yw_0}{w^2}\exp\left(-\frac{r^2}{w^2}\right)\cos(\phi_G^{(1)}), \tag{16d}$$

$$E_y=B_x=0, \tag{16e}$$

where $\phi_G=\omega_0t-k_0z+\tan^{-1}(z/z_R)-zr^2/z_Rw^2-\phi_0$, $\phi_G^{(1)}=\phi_G+\tan^{-1}(z/z_R)$, $w=w_0\sqrt{1+z^2/z_R^2}$ is the beam waist at longitudinal position z, and ϕ_0 is an arbitrary constant. Note

that the symmetrization has no effect on these terms. It modifies terms of order greater than or equal to 2.

As a first approximation, the fields of a laser pulse can be obtained by multiplying expressions (7) or (16) by an envelope factor $f(z-ct)$. However, ultraintense pulses are also short, and therefore not exactly monochromatic. We will now focus on the corrections arising from this effect.

B. Finite pulse duration effects

Let us first compute an estimate of the pulse duration for which these finite pulse duration corrections may be needed. We will go back to the wave equation (9) for fields in vacuum. This can be solved order by order in ϵ [14], which for the fields gives an expansion similar to Eq. (15). We express the electric field as

$$\mathbf{E}=\mathbf{E}(\mathbf{r})e^{ik_0(z-ct)}f(z-ct), \tag{17}$$

where f is again the pulse envelope of width $c\Delta\tau$, and k_0 the average wave vector of the pulse. Inserting this expression in Eq. (9) results in

$$f\Delta\mathbf{E}+2ikf\frac{\partial\mathbf{E}}{\partial z}+2\frac{\partial f}{\partial z}\frac{\partial\mathbf{E}}{\partial z}=\mathbf{0}. \tag{18}$$

We now change of variables from (x,y,z) to $(\xi=x/w_0,\eta=y/w_0,\zeta=z/l)$, where $l=k_0w_0^2$, and focus on the perpendicular component (the component perpendicular to the main direction of propagation z)

$$\left[\left(\frac{\partial^2}{\partial\xi^2}+\frac{\partial^2}{\partial\eta^2}\right)+2i\frac{\partial}{\partial\zeta}+\epsilon^2\frac{\partial^2}{\partial\zeta^2}+2\epsilon^2\frac{1}{f}\frac{\partial f}{\partial\zeta}\frac{\partial}{\partial\zeta}\right]\mathbf{E}_\perp=\mathbf{0}, \tag{19}$$

where as above $\epsilon=1/k_0w_0$. The last term in this equation describes the effects of the finite pulse duration. Therefore, a correction to $\mathbf{E}_\perp$ to first order in ϵ will occur as soon as $|2\epsilon^2\partial(\ln f)/\partial\zeta|\gtrsim\epsilon$. In terms of the pulse duration $\Delta\tau$, this condition can be written

$$c\Delta\tau\lesssim 4\epsilon z_R=2w_0. \tag{20}$$

For a $w_0=10$ μm pulse, this is equivalent to $\Delta\tau\lesssim 60$ fs. This is easily obtained in typical ultrashort lasers, which motivates us in considering this finite pulse size effect.

We will proceed by another order by order derivation, but with the small parameter $\sigma=\lambda_0/c\Delta\tau\ll 1$. We go back to the angular spectrum method, that we generalize as in Ref. [22]; that is, we write

$$E_x(x,y,z=0,t)=E_0(x,y)f(t)\exp(-i\omega_0t), \tag{21}$$

where $f(t)$ is as above the temporal envelope of the pulse, and $E_0(x,y)=E_0\exp[-(x^2+y^2)/w_0^2]$. The time Fourier transform of this expression yields

$$E_x(x,y,z=0,\omega)=E_0(x,y)\tilde{f}(\omega-\omega_0), \tag{22}$$

where $\tilde{f}(\omega)$ is the Fourier transform of $f(t)$. We can use the angular spectrum method for each frequency ω (and wave vector $k=\omega/c$) in the pulse, and write

$$\tilde{E}_x(p,q,\omega)=\tilde{f}(\omega-\omega_0)\frac{1}{\lambda^2}\int\int E_0(x,y)e^{-ik(px+qy)}dx\,dy, \tag{23}$$

where $\lambda=2\pi c/\omega$. Then

$$E_x(x,y,z,t)=\int d\omega\; e^{-i\omega t}\int\int dp\;dq\;\tilde{E}_x(p,q,\omega)e^{ik(px+qy+mz)}. \tag{24}$$

One then remarks that $\tilde{E}_x(p,q,\omega)$ is simply the expression of Eq. (2) multiplied by the envelope in frequency $\tilde{f}(\omega-\omega_0)$, which can be removed from the integral in (p,q). This last integral can be expressed as in Eq. (13) in the form $e^{ikz}\mathcal{E}(x,y,z,\omega)$, so that

$$E_x(x,y,z,t)=\int d\omega\; e^{-i\omega t}e^{ikz}\mathcal{E}(x,y,z,\omega)\tilde{f}(\omega-\omega_0). \tag{25}$$

The important property of $\mathcal{E}$ here is that it is a slowly varying function of ω with respect to the $e^{-i\omega t}$ term. As the pulses we consider are short but still contain many cycles, $\tilde{f}(\omega-\omega_0)$ is sharply peaked around ω_0. These two facts allow us to evaluate Eq. (25) using the standard expansion technique

$$\begin{aligned}E_x(x,y,z,t)&=\mathcal{E}(x,y,z,\omega_0)\int d\omega\; e^{-i\omega(t-z/c)}\tilde{f}(\omega-\omega_0)+\frac{\partial\mathcal{E}}{\partial\omega}(x,y,z,\omega_0)\int d\omega\; e^{-i\omega(t-z/c)}(\omega-\omega_0)\tilde{f}(\omega-\omega_0)+\cdots\\&=\mathcal{E}(x,y,z,\omega_0)e^{ik_0(z-ct)}f(t-z/c)+\frac{\partial\mathcal{E}}{\partial\omega}(x,y,z,\omega_0)e^{ik_0(z-ct)}if'(t-z/c)+\cdots.\end{aligned} \tag{26}$$

The successive derivatives of f are proportional to the successive powers of σ, so that we have obtained the infinite expansion we wanted. Note that the first term corresponds exactly to our expression (7), which justifies *a posteriori* that this is a zero order expression in σ. In the same way, if one develops $\mathcal{E}$ to first order in ϵ in this first term, one recovers expression (16). Eventually, we can obtain the fields to first order in both parameters ϵ and σ (neglecting the terms in $\epsilon\sigma$ as second order) by developing $\mathcal{E}$ to first order in ϵ in the first term and to zero order in the second. This leaves the expressions of E_z and B_z unchanged, but adds a new term to E_x and B_y which writes, for an envelope $f(z-ct)=\cos^2[\pi(t-z/c)/2\Delta\tau]$:

$$E_{x(1)}=\frac{E_0}{2}\sigma\frac{z}{z_R}\left(\frac{w_0}{w}\right)^3\exp\left(-\frac{r^2}{w^2}\right)\times\sqrt{(1-u)^2+(z/z_R)^2}\cos[\pi(t-z/c)/2\Delta\tau]\times\sin[\pi(t-z/c)/2\Delta\tau]\cos(\phi_{G(1)}), \tag{27}$$

$$B_{y(1)}=E_{x(1)}/c, \tag{28}$$

where $u=r^2/w_0^2$, $\phi_{G(1)}=\phi_G+2\tan^{-1}(z/z_R)-\psi$, and ψ is the phase of $1-u+iz/z_R$.

We will finally remark that this method can be applied as well to calculate the vector potential in the Coulomb gauge. Indeed, $\mathbf{A}$ is then given by the wave equation (9) and the gauge condition $\boldsymbol{\nabla}\cdot\mathbf{A}=0$, which is formally equivalent to the Maxwell-Poisson equation $\boldsymbol{\nabla}\cdot\mathbf{E}=0$. Therefore, Eqs. (16a), (16b), and (27) also give an expression for $\mathbf{A}$ in the Coulomb gauge up to first order in ϵ and σ.

III. DERIVATION OF THE RELATIVISTIC PONDEROMOTIVE FORCE

We now give the expression for the ponderomotive force in the relativistic regime and in vacuum. This demonstration closely follows former works by Mora and Antonsen [6,7], who established its expression and validity in the case of a laser propagating in a tenuous plasma.

We use the vector potential in the Coulomb gauge ($\boldsymbol{\nabla}\cdot\mathbf{A}=0$) to describe the laser pulse. As we are in vacuum, the scalar potential is identically equal to zero. As shown at the end of Sec. II, we can write

$$\mathbf{A}=(\tilde{A}^{(0)}_{\perp(0)}+\tilde{A}^{(0)}_{\perp(1)})\mathbf{e}_x+\tilde{A}^{(1)}_{z(0)}\mathbf{e}_z, \tag{29}$$

where the tilde denotes a quantity that is rapidly varying (i.e., at the laser frequency), and where the superscripts are for the expansion according to $\epsilon=1/k_0w_0$, while the subscripts refer to the expansion according to $\sigma=\lambda_0/c\Delta\tau$. To simplify the notations, we write $\tilde{A}^{(0)}_{\perp(0)}=\tilde{A}_\perp$ in the rest of this paper. The equation of motion and the equation of energy conservation for relativistic particles are written

$$\frac{d}{dt}(\mathbf{p}+q\mathbf{A})=(\boldsymbol{\nabla}q\mathbf{A})\cdot\mathbf{v}, \tag{30a}$$

$$\frac{d}{dt}\gamma mc^2=-q\mathbf{v}\cdot\frac{\partial\mathbf{A}}{\partial t}, \tag{30b}$$

where q is the charge and m the mass of the particle.

In the laser frame coordinates, with the new variables $(z,\tau=t-z/c)$, these equations can be written as:

$$\left[\left(1-\frac{v_z}{c}\right)\frac{\partial}{\partial\tau}+\mathbf{v}\cdot\boldsymbol{\nabla}\right](\mathbf{p}+q\mathbf{A})=(\boldsymbol{\nabla}q\mathbf{A})\cdot\mathbf{v}-\frac{q}{c}\left(\mathbf{v}\cdot\frac{\partial\mathbf{A}}{\partial\tau}\right)\mathbf{e}_z, \tag{31a}$$

$$\left[\left(1-\frac{v_z}{c}\right)\frac{\partial}{\partial\tau}+\mathbf{v}\cdot\boldsymbol{\nabla}\right]\gamma mc^2=-q\mathbf{v}\cdot\frac{\partial\mathbf{A}}{\partial\tau}. \tag{31b}$$

A last manipulation will give us our starting equations. We reduce the first equation to its two components perpendicular to the direction of propagation of the pulse, and as a second equation we take the axial component of Eq. (31a) minus Eq. (31b), divided by the speed of light:

$$\left[\left(1-\frac{v_z}{c}\right)\frac{\partial}{\partial\tau}+\mathbf{v}\cdot\boldsymbol{\nabla}\right](\mathbf{p}_\perp+q\mathbf{A}_\perp)=(\boldsymbol{\nabla}_\perp q\mathbf{A})\cdot\mathbf{v}, \tag{32a}$$

$$\left[\left(1-\frac{v_z}{c}\right)\frac{\partial}{\partial\tau}+\mathbf{v}\cdot\boldsymbol{\nabla}\right](p_z+qA_z-\gamma mc)=q\mathbf{v}\cdot\frac{\partial\mathbf{A}}{\partial z}. \tag{32b}$$

We then perform an order by order expansion based on the small parameters ϵ and σ. In the vicinity of the focus, the expression of the vector potential shows us that the various derivatives scale as $\boldsymbol{\nabla}_\perp\sim 1/w_0\sim\epsilon/\lambda_0$, $\partial/\partial z\sim 1/z_R\sim\epsilon^2/\lambda_0$, and $\partial/c\partial\tau=\partial/c\partial\tau_0+\partial/c\partial\tau_1$, where $\partial/c\partial\tau_0$ is related to the fast oscillations at the laser frequency and scales as $1/\lambda_0$, while $\partial/c\partial\tau_1$ is related to the temporal envelope of the pulse and scales as $1/c\Delta\tau\sim\sigma/\lambda_0$. As both parameters ϵ and σ are required to evaluate the derivatives, an order by order derivation of the ponderomotive force will be *a priori* possible provided that $\sigma\sim\epsilon$, which for a $\lambda_0=1\,\mu$m and $w_0=10\,\mu$m pulse implies $\Delta\tau\sim 200$ fs. In the same way, we write all quantities f as $f=\tilde{f}+\overline{f}$, where $\tilde{f}$ is the rapidly varying part of f and $\overline{f}$ the slowly varying part with respect to the laser frequency.

Let us first remark that the term $1-v_z/c$ appears in both equations. We will suppose it to be a zero order quantity in the rest of the calculation, that is $1-v_z/c\gg\epsilon\sim\sigma$. This is an essential requirement for this derivation to be valid. The zero order part of Eq. (32b) reads

$$\frac{\partial}{\partial\tau_0}(p_z-\gamma mc)=0, \tag{33}$$

where we note the zero order quantities with no indices. We can then conclude that the quantity $p_z-\gamma mc$ varies slowly with respect to the wave frequency, so that $p_z-\gamma mc=\overline{p_z}-\overline{\gamma mc}$. In the same way, the lowest order part of Eq. (32a) reads

$$\frac{\partial}{\partial\tau_0}(\mathbf{p}_\perp+q\mathbf{A}_\perp)=0. \tag{34}$$

This allows us to write

$$\mathbf{p}_\perp=\tilde{\mathbf{p}}_\perp+\overline{\mathbf{p}}_\perp, \tag{35}$$

where

$$\tilde{\mathbf{p}}_\perp = -q\tilde{\mathbf{A}}_\perp \tag{36}$$

is the zero-order oscillation momentum of the electron in the laser field. We then consider the first order part of Eq. (32a) in both parameters ϵ and σ. After multiplication by γmc, it reads

$$\begin{aligned}(\overline{\gamma}mc-\overline{p_z})\frac{\partial}{\partial\tau_0}(\mathbf{p}_\perp^{(1)}+\mathbf{p}_{\perp(1)}+\mathbf{A}_{\perp(1)})\\ +(\overline{\gamma}mc-\overline{p_z})\frac{\partial}{\partial\tau_1}(\overline{\mathbf{p}}_\perp)+c(\mathbf{p}_\perp\cdot\boldsymbol{\nabla}_\perp)\overline{\mathbf{p}}_\perp\\ =c(\boldsymbol{\nabla}_\perp q\mathbf{A})\cdot\mathbf{p}.\end{aligned} \tag{37}$$

We next average over the fast time scale, and this equation simplifies to

$$(\overline{\gamma}mc-\overline{p_z})\frac{\partial}{\partial\tau_1}(\overline{\mathbf{p}}_\perp)+c(\overline{\mathbf{p}}_\perp\cdot\boldsymbol{\nabla}_\perp)\overline{\mathbf{p}}_\perp=c\overline{(\boldsymbol{\nabla}_\perp q\mathbf{A})\cdot\mathbf{p}}. \tag{38}$$

We then make use of Eqs. (29) and (36) to express the last term at lowest order in the form

$$\overline{(\boldsymbol{\nabla}_\perp q\mathbf{A})\cdot\mathbf{p}}=-\tfrac{1}{2}\boldsymbol{\nabla}_\perp\overline{|q\tilde{\mathbf{A}}_\perp|^2}. \tag{39}$$

We now establish an expression for the fast scale averaged relativistic factor. Again using Eq. (36), we can write

$$\gamma^2=1+\frac{1}{m^2c^2}[|\overline{\mathbf{p}}_\perp-q\tilde{\mathbf{A}}_\perp|^2+p_z^2]. \tag{40}$$

Using the equality $p_z=\overline{p_z}+mc(\gamma-\overline{\gamma})$ and averaging over the fast time scale, we obtain

$$\overline{\gamma^2}=1+\frac{1}{m^2c^2}[|\overline{\mathbf{p}}_\perp|^2+\overline{p_z^2}+\overline{|q\tilde{\mathbf{A}}_\perp|^2}]. \tag{41}$$

With this expression, we can define an averaged velocity in the form $\overline{\mathbf{v}}=\overline{\mathbf{p}}/\overline{\gamma}m$. Putting together this definition and Eq. (39), we can write Eq. (38) as

$$\left[\left(1-\frac{\overline{v_z}}{c}\right)\frac{\partial}{\partial\tau_1}+\overline{\mathbf{v}}_\perp\cdot\boldsymbol{\nabla}_\perp\right]\overline{\mathbf{p}}_\perp=-\frac{1}{2m\overline{\gamma}}\boldsymbol{\nabla}_\perp\overline{|q\tilde{\mathbf{A}}_\perp|^2}. \tag{42}$$

This constitutes the first order averaged equation of motion in the transverse direction, the last term being precisely the ponderomotive potential.

We now give a sketch of the demonstration of the equivalent equation for the longitudinal direction. At first order, and after multiplication by γmc and averaging over the fast time scale, Eq. (32b) is written

$$\begin{aligned}\left[(\overline{\gamma}mc-\overline{p_z})\frac{\partial}{\partial\tau_1}+c(\overline{\mathbf{p}}_\perp\cdot\boldsymbol{\nabla}_\perp)\right]\overline{p_z}\\ =\left[(\overline{\gamma}mc-\overline{p_z})\frac{\partial}{\partial\tau_1}+c(\overline{\mathbf{p}}_\perp\cdot\boldsymbol{\nabla}_\perp)\right]\overline{\gamma}mc.\end{aligned} \tag{43}$$

The derivation of Eq. (41) with respect to τ_1 yields

$$\frac{1}{2}\frac{\partial}{\partial\tau_1}\overline{|q\tilde{\mathbf{A}}_\perp|^2}=\overline{\gamma}mc\frac{\partial}{\partial\tau_1}\overline{\gamma}mc-\overline{p}_z\frac{\partial}{\partial\tau_1}\overline{p}_z-\frac{1}{2}\frac{\partial}{\partial\tau_1}|\overline{\mathbf{p}}_\perp|^2. \tag{44}$$

Multiplying Eq. (42) by $\overline{\mathbf{p}}_\perp$, and Eq. (41) by $\overline{\mathbf{p}}_\perp\cdot\boldsymbol{\nabla}_\perp$, combining the two results and using Eq. (43), we obtain

$$-\frac{1}{2}\frac{\partial}{\partial\tau_1}|\overline{\mathbf{p}}_\perp|^2=c(\overline{\mathbf{p}}_\perp\cdot\boldsymbol{\nabla}_\perp)\overline{\gamma}mc+\overline{p}_z\frac{\partial}{\partial\tau_1}(\overline{p}_z-\overline{\gamma}mc). \tag{45}$$

These two last equations allow us to rewrite the second term in Eq. (43), so that finally:

$$\left[\left(1-\frac{\overline{v_z}}{c}\right)\frac{\partial}{\partial\tau_1}+\overline{\mathbf{v}}_\perp\cdot\boldsymbol{\nabla}_\perp\right]\overline{p}_z=-\frac{1}{2m\overline{\gamma}}\left(-\frac{1}{c}\frac{\partial}{\partial\tau_1}\overline{|q\tilde{\mathbf{A}}_\perp|^2}\right), \tag{46}$$

which is precisely the longitudinal equivalent of Eq. (42) that we were looking for.

We terminate this calculation by reintroducing in Eqs. (42) and (46) two second order terms, namely, $\overline{v_z}\partial/\partial z$ in the left term of both equations and $(-1/2m\overline{\gamma})\partial/\partial z\overline{|q\tilde{\mathbf{A}}_\perp|^2}$ in the right term of Eq. (46), so that the averaged equation of motion of the electron in the laboratory frame finally writes:

$$\frac{d\overline{\mathbf{p}}}{dt}=-\frac{1}{2m\overline{\gamma}}\boldsymbol{\nabla}\overline{|q\tilde{\mathbf{A}}_\perp|^2}. \tag{47}$$

This, together with Eq. (41), constitutes the relativistic generalization of the ponderomotive force. It has been derived for a linearly polarized laser [see Eq. (29)], but this derivation can be easily generalized for the case of an arbitrary polarization. We recover the main feature of the nonrelativistic case: the charged particle is expelled from the regions of high field intensity in the direction of the gradient. In the case of a linearly polarized wave, the direction of polarization plays no particular role, which contradicts the results of Ref. [10].

At this point, we can affirm that this expression is valid provided that (i) the considered particle has a relatively slow speed in the z direction, so that $1-v_z/c\gg\epsilon$ and $\gg\sigma$; (ii) ϵ and σ are of the same order; and (iii) it is possible to reintroduce the two second order terms that we added to write Eq. (47). Condition (i) seems *a priori* the most stringent one. We will check the importance of these conditions with numerical simulations in Sec. IV.

We conclude this section by comparing our expression with similar ones derived by other authors. Bauer, Mulser, and Steeb [5] used a Hamiltonian formalism to derive an expression of the ponderomotive potential in the relativistic regime. Their analysis supposed that it is possible to define an oscillation center for the motion of the particle. They did not specify the physical conditions under which such an assumption is valid. If we write $\tilde{\mathbf{A}}_\perp=\hat{\mathbf{A}}_\perp e^{ik_0(z-ct)}+\text{c.c.}$, then $\overline{|q\tilde{\mathbf{A}}_\perp|^2}=2|q\hat{\mathbf{A}}_\perp|^2$. We define the effective mass $m_{\text{eff}}=m(1+2q^2|\hat{\mathbf{A}}_\perp|^2/m^2c^2)^{1/2}$ [2], and Eq. (47) can be written

$$\frac{d\overline{\mathbf{p}}}{dt} = -\frac{c^2}{\gamma_0}\boldsymbol{\nabla} m_{\mathrm{eff}}, \tag{48}$$

where $\gamma_0 = (1-\overline{v^2}/c^2)^{-1/2}$ so that $\gamma_0 m_{\mathrm{eff}} = m\overline{\gamma}$ in our notations. This equation is similar to Eqs. (11) and (12) of Ref. [5]. Startsev and McKinstrie [8] used a covariant formalism, and assumed that the amplitude of the wave varies slowly with respect to the phase. They supposed that these relative variation rates can be described by a single parameter ϵ that they did not relate to any physical quantity. They recovered the expression for the relativistic ponderomotive force [their Eq. (3.7)] in terms of the proper time, which had already been obtained in a different way by Schmidt and Wilcox [4].

IV. TEST-PARTICLE SIMULATIONS

A. Description and test of the program

In order to test the validity of the RPF [Eq. (47)], we designed a 3D test-particle simulation program. It computes the trajectory of individual electrons in the field of a laser near focus, using either the Lorentz equation or the RPF. More precisely, the electron is moved by numerically solving the differential equations $d\mathbf{r}/dt = \mathbf{p}/m\gamma$ and $d\mathbf{p}/dt = \mathbf{f}(\mathbf{r},\mathbf{p},t)$, using an adaptative Runge-Kutta method [23]. We used four different methods of calculation: the first one is based on the relativistic ponderomotive description, while the three others solve the equations of motion in the rapidly varying fields, within three different approximations. More precisely, we proceed as follows.

(1) All quantities are time averaged quantities, in particular $\gamma = \overline{\gamma}$ [Eq. (41)], and **f** is the RPF [Eq. (47)]. Then, as a zero order vector potential used to define the ponderomotive force, we take the expression of Eq. (16a), which describes A as well, as shown at the end of Sec. II.

(2) γ is the usual Lorentz factor and **f** the Lorentz force, where **E** and **B** are the zero order fields used in Refs. [9] and [10], i.e., Eqs. (16a) and (16c).

(3) Like (2), but with the fields correct up to first order in ϵ and σ, i.e., Eqs. (16) and (27).

(4) Like (2), but with the fields correct up to all orders in ϵ and order zero in σ, that is Eq. (7). These fields will be referred to as the ''exact'' fields, though finite duration effects are not included. We will see indeed that in all the cases we study in this paper, the approximation on which they are based is relevant. These fields are evaluated by numerical integration, and are very expensive in terms of computing time, which explains the relatively small number of simulations we have been able to perform.

We will use these numbers to refer to these different methods to calculate the electron motion. All our simulations consider a linearly polarized laser of wavelength $\lambda_0 = 1\ \mu$m, with the electric field in the x direction and the magnetic field in the y direction. As in Refs. [9] and [10], we study electrons with an initial velocity in the direction of propagation of the laser pulse, which has a finite duration and a sine squared shape, namely, $f(z-ct) = \cos^2[\pi(t-z/c)/2\Delta\tau]$. We start the simulation at the moment when the leading edge of the pulse reaches the electron, and we compute the electron motion up to the point where the laser pulse has overtaken it. We normalize the laser amplitude in the usual way, $a = eE_0/mc\omega_0$, so that $a = 0.85$ corresponds to an intensity $I = 10^{18}$ W cm^{-2} for a $\lambda_0 = 1\ \mu$m wavelength. We also normalize the electron momentum to mc. Our reference frame is centered at focus, so that the focal point coordinates are (0,0,0). The laser pulse is propagating in the $+z$ direction.

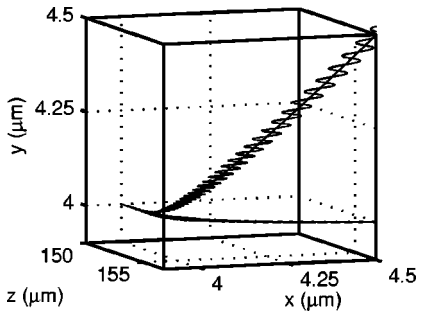

FIG. 1. Electron trajectory calculated by methods (1), (2), and (3). Parameters are $a = 0.3$, $\Delta\tau = 200$ fs, $w_0 = 10\ \mu$m, $p_{z0} = 0.1$, and $z_0 = 150\ \mu$m. With methods (1) (ponderomotive force) and (3) (first order fields), the electron trajectory (the two curves in the upper part of the figure) is along the field intensity gradient, whereas the zero order fields [method (2)] confine the electron in the plane of polarization of the pulse.

We checked our program with simulations in the nonrelativistic regime, where the validity of the ponderomotive force is well established [24–28]. In the limit $\gamma \to 1$, Eq. (47) reduces to the well-known equation (1). Cicchitelli, Hora, and Postle [18] showed that the higher order terms in ϵ were necessary to describe the electron motion in this regime correctly, and that the zero order fields lead to an erroneous anisotropic electron motion. Our numerical conditions are $a = 0.3$ ($I = 1.2\times10^{17}$ W cm^{-2}), $\Delta\tau = 200$ fs, $w_0 = 10\ \mu$m, and $p_{z0} = 0.1$, where p_{z0} is the electron initial momentum. With these values, $\epsilon \simeq \sigma \simeq 1.6\times10^{-2}$.

Figure 1 shows the trajectory of an electron initially at $x_0 = y_0 = 4\ \mu$m and $z_0 = 150\ \mu$m as calculated by methods (1), (2), and (3). Exactly as expected, the motion with the zero order fields [method (2)] is restricted to the plane of polarization of the pulse, and is therefore nonisotropic. Conversely, the inclusion of the first order corrections [method (3)] leads to a very good agreement with the ponderomotive force calculation [method (1)].

The average ponderomotive motion of the electron takes its source in two effects. First, the zero order motion of the electron is simply the oscillation in the x direction due to E_x. This causes it to explore the gradient of E, which causes on the average its drift and acceleration in the x direction. This is precisely the usual explanation of the ponderomotive motion for purely electrostatic fields. The force is proportional to $\boldsymbol{\nabla}_\perp E$, and is therefore of order ϵ. Second, the field B_z is almost in phase with the zero order velocity v_x of the electron, as can be deduced from the set of equations (16). The force $v_x \times B_z$ has then a nonvanishing average which causes the drift in the y direction. This force is again of order ϵ due to B_z. Note that the field E_z has almost no effect on the electron motion in this case, as can be checked by suppressing it artificially.

As $c\Delta\tau > 2w_0$ here, we expect the first order correction in σ to play no role. We checked this again by suppressing this term in the expression of the first order fields: we found no

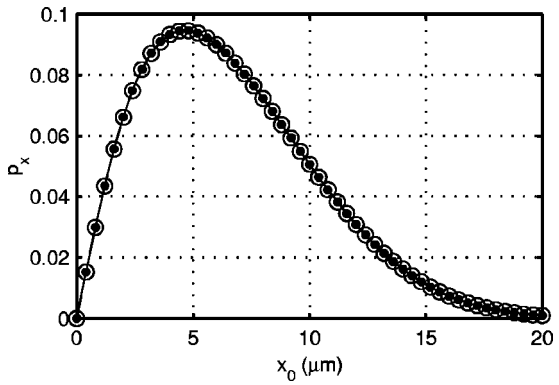

FIG. 2. Final p_x as a function of the initial position x_0 of the electron. Parameters as in Fig. 1. The solid line corresponds to results obtained with the exact fields [method (4)], the open circles are the result of the first order fields, and the dots correspond to the motion calculated with the ponderomotive force [method (1)].

differences, which confirms that the finite pulse duration effects can be neglected here. We will come back to this point later in this section.

In order to compare more precisely the different calculations, in Fig. 2 we plot the final p_x, and in Fig. 3 the final p_z, as functions of the initial position along the x axis, with $z_0=150$ μm. The solid line corresponds to the exact fields [method (4)], the open circles to the first order fields [method (3)], and the dots to the RPF [method (1)]. Note also that the curve $p_y(y_0)$ would be exactly the same as Fig. 2. All three curves coincide very precisely in Fig. 2, but a clear disagreement appears in Fig. 3 between the RPF and the first order fields. As finite pulse size effects are of no concern here, we can affirm that method (4) gives the exact electron motion in this case. We conclude that the first order fields are insufficient to describe the longitudinal electron motion with good accuracy. Higher order terms are needed, and then give a very good agreement with the RPF. This gives us the answer to one of the points we raised in discussing the validity of Eq. (47): it is possible to reintroduce the two second order terms we mentioned, which are precisely related to the longitudinal part of the motion. An expression of the fields up to second order would probably have been sufficient in this

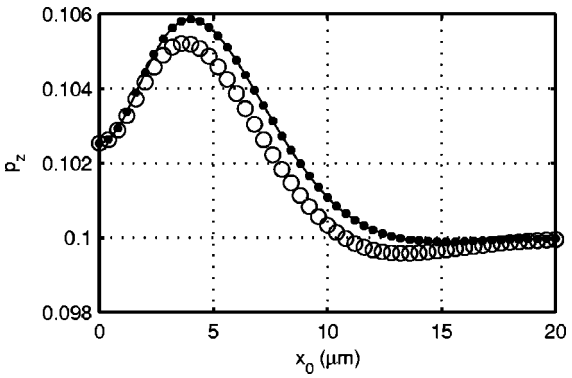

FIG. 3. Final p_z as a function of the initial position x_0 of the electron, with the same parameters as in Fig. 1. The solid line corresponds to results obtained with the exact fields [method (4)], the open circles are the result of the first order fields, and the dots correspond to the motion calculated with the ponderomotive force.

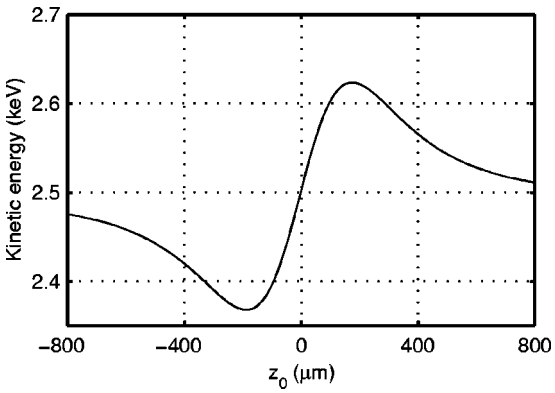

FIG. 4. Kinetic energy of the scattered electron as a function of its initial longitudinal position, with $x_0=y_0=0$. The parameters are as in Figs. 1, 2, and 3. The electron motion is calculated with method (4) (exact fields).

case, but as we wanted to study the electron motion in the highly relativistic regime of Hartemann *et al.*, where the validity of the RPF is not obvious, we preferred to compute the full expression of the fields.

Finally, Fig. 4 shows the final kinetic energy of the electron as a function of its initial longitudinal position, with $x_0=y_0=0$. Method (4) has been used here. One clearly sees the effect of the longitudinal ponderomotive force, which accelerates the electrons initially after focus and decelerates the electrons initially before focus. This is due to the fact that the electron ''sees'' the ascending (descending) part of the pulse at a position closer to focus than the descending one (ascending). The effect of diffraction of the laser wave then makes the ascending (descending) gradient stronger than the descending (ascending) one.

Let us now check the second point in the validity of the RPF, that is the fact that ϵ should be of the order of σ for Eq. (47) to be correct. Here we show the results of two simulations, one with $\epsilon\sim\sigma^2$ and the other with $\sigma\sim\epsilon^2$. Figure 5 is a plot of the final p_x as a function of the initial position x_0 for a case where $a=0.1$, $p_{z0}=0.1$, $z_0=-100$ μm, $w_0=9.5$ μm ($\epsilon=1.7\times10^{-2}$), and $\Delta\tau=6$ ps ($\sigma=5.6\times10^{-4}$). The agreement between the values calculated by the RPF (circles) and method (4) (exact fields) is excellent. For the electron at $x_0=0$, it is not scattered by the ponderomotive

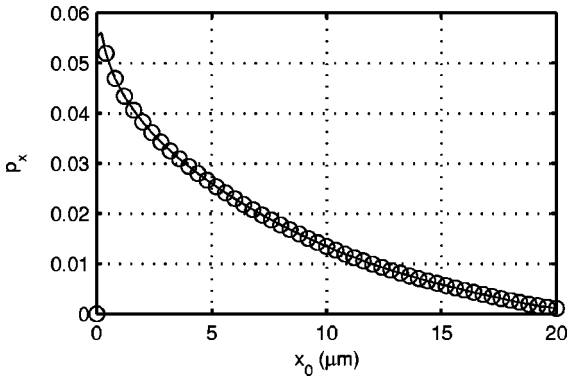

FIG. 5. Final p_x as a function of the initial position x_0 of the electron. Parameters are $a=0.1$, $\Delta\tau=6$ ps, $w_0=9.5$ μm, $p_{z0}=0.1$, and $z_0=-100$ μm. The solid line corresponds to method (4) (exact fields), while the circles refer to the RPF.

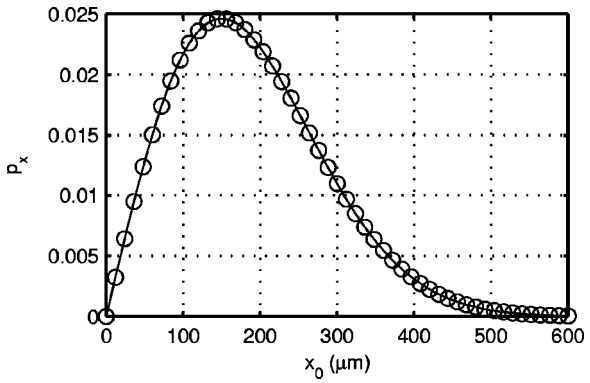

FIG. 6. Final p_x as a function of the initial position x_0 of the electron. Parameters are $a=0.7$, $\Delta\tau=200$ fs, $w_0=300$ μm, $p_{z0}=0.1$, and $z_0=100$ μm. The solid line corresponds to the RPF, while the circles refer to method (4) (exact fields).

force as expected, but, as this initial position is unstable, the finite machine precision causes the expulsion of the electron when its motion is calculated with the exact fields. In the same way, Fig. 6 shows the final p_x as a function of the initial position x_0 for the values $a=0.7$, $p_{z0}=0.1$, $z_0=100$ μm, $w_0=300$ μm ($\epsilon=5.3\times10^{-4}$), and $\Delta\tau=200$ fs ($\sigma=1.7\times10^{-2}$). Here again, we see an excellent agreement between the two calculations. This allows us to conclude that the validity is in fact much wider than expected.

We now come back to the finite pulse duration effects. The previous results agree with our estimate [Eq. (20)] of $\Delta\tau$, for which the first order correction in σ is needed. To confirm the validity of this estimate, we performed a simulation with $w_0=10$ μm and $\Delta\tau<60$ fs, namely, $\Delta\tau=12$ fs. The other parameters are $a=0.3$, $z_0=-40$ μm, and $p_{z0}=0.1$. The simulation is made twice, once with the corrections in σ and another time without this correction. We can see in Fig. 7 that the two simulations are in slight disagreement, as expected. We conclude that our estimate was correct and that the finite pulse size corrections are not needed when $c\Delta\tau>2w_0$. All our computations in the following are performed with $c\Delta\tau\gg2w_0$, so that method (4) can be considered as giving the *exact* electron motion, as has been stated above.

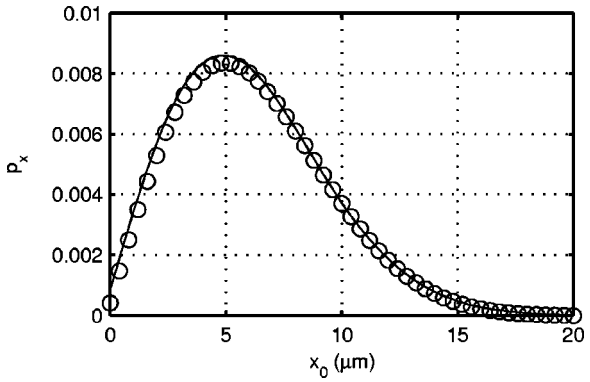

FIG. 7. Final p_x as a function of the initial position x_0 of the electron. Parameters are $a=0.3$, $\Delta\tau=12$ fs, $w_0=10$ μm, $p_{z0}=0.1$, and $z_0=-40$ μm. Both curves correspond to trajectories calculated with the first order corrections in ϵ, but with the first order correction in σ (solid line) or without it (circles).

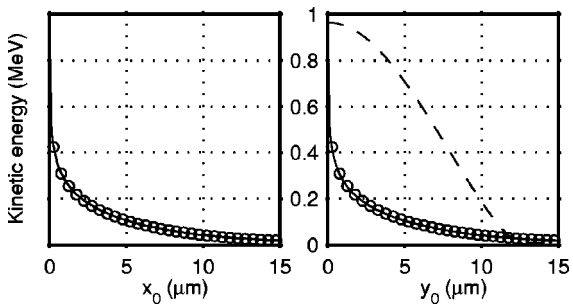

FIG. 8. Final energies of the scattered electrons as a function of their initial transverse position. Parameters are $a=3$, $\Delta\tau=400$ fs, $w_0=10$ μm, $v_{z0}=0.2c$, and $z_0=-160$ μm. The solid line corresponds to the values obtained with the exact fields [method (4)], and the circles to the values obtained with the RPF. The broken line on the right is the value as calculated with the model of Ref. [10] [model (2)].

B. RPF with initially slow electrons

Let us now come back to the point we raised in Sec. I, and which motivated this paper, that is the disagreement between the RPF and the recent papers by Malka, Lefebvre, and Miquel [10] and Hartemann *et al.* [9]. The results in these two papers share the fact that the laser intensity is relativistic, $a>1$, but Hartemann *et al.* also considered electrons which are initially in the relativistic regime ($\gamma\gg1$) whereas the authors of Ref. [10] studied the acceleration of initially ''slow'' electrons ($\gamma\simeq1$). This second regime is closer to the one we have just studied, so we will start with it.

In Ref. [10] the authors reported on an experiment where free electrons have been accelerated in vacuum by a high-intensity ($I\simeq10^{19}$ W cm^{-2}, $a=3$), short ($\Delta\tau=400$ fs) linearly polarized laser pulse. The electrons' initial velocity is around $0.1c$. The focal spot waist is $w_0=10$ μm, so that $\epsilon\simeq1.6\times10^{-2}\ll1-v_{0z}/c$. This regime of parameters differs from the previous one only in the fact that the laser intensity is higher. Therefore, we expect the RPF still to be valid. The simulation confirms this fact: Fig. 8 shows the final energy for an electron initially along the x (y) axis, with an initial longitudinal position $z_0=-160$ μm and velocity $v_{0z}=0.2c$. The solid line corresponds to method (4), while the circles correspond to the RPF. All four curves are exactly similar, which means that the RPF is perfectly valid in this regime of parameters, and therefore that the scattering is not limited to the (**E**,**k**) plane, as claimed by the authors of Ref. [10]. For comparison, the result given by the zero order fields is shown by the dashed line. It coincides with the two other curves on the left (the electron initially in the plane of polarization), but is in complete disagreement for the electrons initially on the y-z plane. The electron trajectories in this fully relativistic case are similar to the one shown in Fig. 1 [11]. The final energy as a function of z_0 for $x_0=y_0=0$ is slightly affected by the choice of the wrong fields: method (4) gives a curve $\gamma(z)$ very close to Fig. 3 of Ref. [10].

In order to improve the comparison between our simulations and an experiment, we simulated the trajectories of 1000 electrons whose initial position is taken at the same $z_0=-200$ μm, but whose transverse position is chosen randomly using a Gaussian distribution

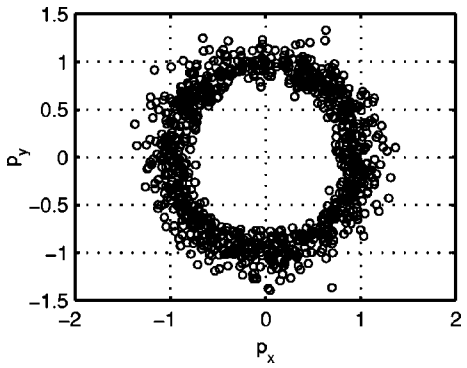

FIG. 9. Final transverse momentum of the electrons for the parameters $a=3$, $\Delta\tau=350$ fs, $w_0=10\ \mu$m, $v_{z0}=0.2c$, and $z_0=-200\ \mu$m. The 1000 electrons are initially distributed randomly using a Gaussian probability, with $r_0=1\ \mu$m (see text). The trajectories are computed with the exact fields, but the RPF gives almost exactly the same points.

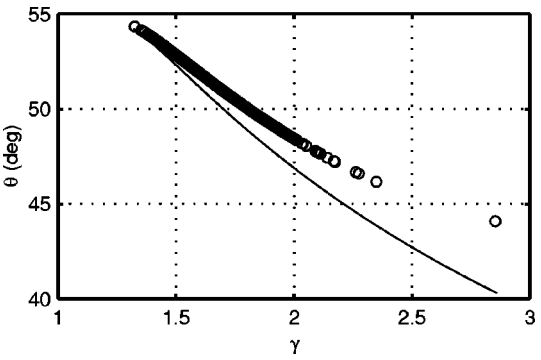

FIG. 10. Ejection angle of the electrons vs their final Lorentz factor. The initial conditions are as in Fig. 9. The open circles correspond to the trajectories computed using the exact fields [method (4)], while the solid line corresponds to theoretical formula (50). The point on the right corresponds to an electron initially on axis.

$$\mathcal{P}(x,y)=\frac{1}{2\pi r_0^2}e^{-(x^2+y^2)/2r_0^2},$$

with $r_0=1\ \mu$m. All electrons have the same initial velocity $v_{0z}=0.2c$. The laser pulse has the same parameters as above, except for the duration $\Delta\tau=350$ fs, which causes no important differences. Figure 9 shows the final $\mathbf{p}_\perp$ of the electrons as calculated by method (4). It is striking evidence of the isotropy of the scattering: the electrons are emitted exactly in the same way in the x direction (direction of polarization) and in the y direction. The RPF gives results in very good agreement with Fig. 9. We checked this point numerically by computing an estimate of the deviation from the ponderomotive motion, in the form

$$\sigma(\delta p)=\sqrt{\langle\delta p^2\rangle-\langle\delta p\rangle^2},$$

where the mean value $\langle\ \rangle$ refers to our 1000 trajectories. Here δp is $\delta p=(p_{\mathrm{EX}}-p_{\mathrm{RPF}})/\overline{p_{\mathrm{EX}}}$, where p is one of the three components of the final electron momentum (p_x, p_y, or p_z), p_{EX} means the value obtained with the exact fields, p_{RPF} means the value obtained with the RPF, and $\overline{p_{\mathrm{EX}}}$ is $\sqrt{\langle p_{\mathrm{EX}}^2\rangle}$ for p_x and p_y, and $\overline{p_{\mathrm{EX},z}}=\sqrt{\langle(p_{\mathrm{EX},z}-p_{0z})^2\rangle}$. As a reference, we also give the values obtained in the nonrelativistic case: $a=0.3$, $w_0=10\ \mu$m, $\Delta\tau=350$ fs, $v_{0z}=0.1c$, $z_0=-200\ \mu$m, and $r_0=1\ \mu$m. All the values are reported in Table I. We can see that the difference between the RPF and the exact electron motion has slightly increased in the case $a=3$, but the various $\sigma(\delta p)$'s are still at sufficiently low values to conclude on the validity of the RPF in this regime.

Another interesting characteristic of the ponderomotive motion is the fact that the final energy of the particle and its escape angle θ (the angle between its trajectory and the laser axis) are linked, or, equivalently, that the longitudinal and transverse parts of the momentum are connected. It is usually assumed that the plane wave relation is valid, that is, $p_z=p_\perp^2/2$ or

$$\cos(\theta)=\sqrt{\frac{\gamma-1}{\gamma+1}} \tag{49}$$

for an electron initially at rest. This relation may be demonstrated in two cases, either using the quasistatic approximation in which the fields are supposed to depend on z and t only in the combination $\tau=t-z/c$ [7], or with the fields of order zero in ϵ [9], where it is a direct consequence of the facts that $B_y=E_x/c$ and that the other fields are equal to zero. Here, however, none of these two approximations are made, so that the relation we obtain is different from the above one, as can be seen in Fig. 10 which shows the ejection angle θ as a function of the final electron Lorentz factor γ for the simulation with the exact fields and the RPF model (open circles), and as calculated by the theoretical relation

$$\theta=\tan^{-1}\left[\frac{\sqrt{2(\gamma/\gamma_0-1)/(1+\beta_0)}}{\gamma-\gamma_0(1-\beta_0)}\right] \tag{50}$$

(solid line), which is the equivalent of Eq. (49) for electrons with initial energy γ_0, and $\beta_0=p_{z0}/\gamma_0$ [9]. The authors of Ref. [10] supposed that relation (50) was valid, and had some difficulties in explaining their experimental results.

TABLE I. Numerical estimation of the difference between the motion calculated by the exact fields and by the RPF. For the definition of σ, see the text. In all cases, $\Delta\tau=350$ fs.

a	w_0 (μm)	z_0 (μm)	v_{z0}/c	$\sigma(\delta p_x)$	$\sigma(\delta p_y)$	$\sigma(\delta p_z)$
0.3	10.0	-200	0.1	1.9×10^{-3}	9.7×10^{-4}	6.4×10^{-5}
3.0	10.0	-200	0.2	2.9×10^{-3}	2.0×10^{-3}	6.6×10^{-4}
10.0	10.0	-200	0.1	6.9×10^{-3}	4.7×10^{-3}	2.0×10^{-3}
5.34	4.95	-15×10^3	0.99 [a]	1.2×10^{-1}	9.3×10^{-2}	5.6×10^{-1}

[a] $\gamma_0=10$.

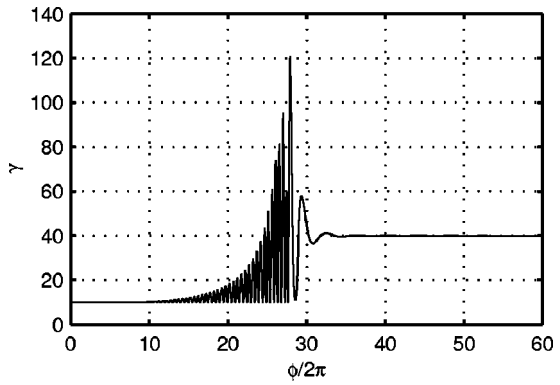

FIG. 11. Evolution of the γ factor of the electron as a function of its phase relative to the pulse envelope, the trajectory being computed using the zero order fields. The parameters are $a=3.41$, $w_0=20$ μm, $\Delta\tau=100$ fs, $\gamma_0=10$, and $z_0=-7.6$ mm.

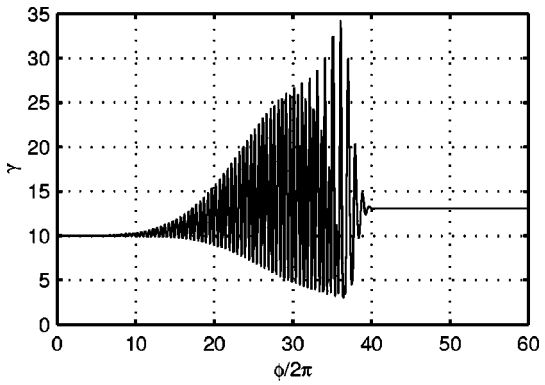

FIG. 12. Evolution of the γ factor of the electron as a function of its phase relative to the pulse envelope, the trajectory being computed using the exact fields [method (4)]. The parameters are as in Fig. 11.

The correction to this formula that we demonstrate here may help, but as the experimental laser pulse is probably quite different from the one we simulate, it is unlikely that a perfect agreement can be reached in any case.

We can conclude that the experimental results reported in Ref. [10] are puzzling, as they are in strong disagreement with one important point of the simulations above, namely, the fact that the scattering is isotropic. The results are interesting in the sense that they represent the first experimental observation of electrons accelerated by the ponderomotive force in vacuum to such high energies. However, the authors' claim that no electron was observed in the direction perpendicular to the direction of polarization really needs to be explained. A more precise experiment would be of great interest in this context.

We now go to more relativistic regimes. As we are expecting the condition $1-v_z/c \gg \epsilon$ to be determinant in the validity of the RPF, we first increase a without changing v_{z0}. We have seen that the electrons are pushed forward by the longitudinal part of the RPF, which increases their longitudinal velocity. As the laser intensity is raised, v_z will reach high values sooner and sooner in the pulse profile, so that the agreement between the exact motion and the RPF is likely to diminish. This is confirmed by a simulation at $a=10$ ($I=1.4\times10^{20}$ W cm^{-2}), with $w_0=10$ μm, $\Delta\tau=350$ fs, $v_{0z}=0.1c$, $z_0=-200$ μm, and $r_0=1$ μm. The scattering is still very close to perfect isotropy, but the numerical deviation from the RPF has increased again, as can be seen in Table I. The values of all $\sigma(p)$ are, however, under 1%, so that we can conclude that the RPF is a valid description of the electron motion for electrons initially slow ($1-v_z/c \gg \epsilon$) up to extremely high values of the laser intensity. The very long computation time needed when using the exact fields has prevented us from studying more precisely this limit.

C. Interaction with highly relativistic electrons

We finally consider the case of initially highly relativistic electrons. This corresponds to the regime studied by Hartemann *et al.* [9]. Using a zero order description for the fields and a 2D simulation program, these authors concluded that the electrons are scattered with a very high energy (up to $\gamma \simeq 250$ for $a=5.34$, $\Delta\tau=800$ fs, $w_0=4.95$ μm, and $\gamma_0=10$). Here again, the correct description of the fields changes the theoretical prediction, but even more dramatically. We first notice a sign mistake in the zero order expression of the fields used in Ref. [9] [Eq. (52) of Ref. [9]]. Indeed, the phase velocity of the light near focus is greater than c [see the definition of ϕ_G in Eq. (16)], whereas Ref. [9]'s expression results in a phase velocity smaller than c. As expected, the effect of this correction is a slight lowering of the maximum energy of the electron, as can be seen in Fig. 11, which shows the evolution of the γ factor of the electron as a function of its phase in the pulse, for the same parameters as Fig. 10 of Ref. [9]. The final Lorentz factor with the zero order fields is now $\gamma\sim40$ instead of $\gamma\sim150$. (We also computed the trajectory with the same erroneous fields as Hartemann *et al.*, and recovered their Fig. 10.) The correct computation (with the fields correct to all orders in ϵ) is even more different, as can be seen in Fig. 12. The inclusion of the longitudinal fields tends to reduce the final energy, which is now $\gamma\sim13$. The corresponding electron trajectory in the x-z plane is plotted in Fig. 13. We can see that the electron is scattered slightly before focus, in a more violent way than in the ponderomotive case of Fig. 1. This is in agreement with Ref. [9]'s description, which insists on the fact that the electron-laser interaction terminates in about a wavelength. Note, however, that the electron quiver amplitude remains smaller than the laser beam waist. Therefore, the explanation

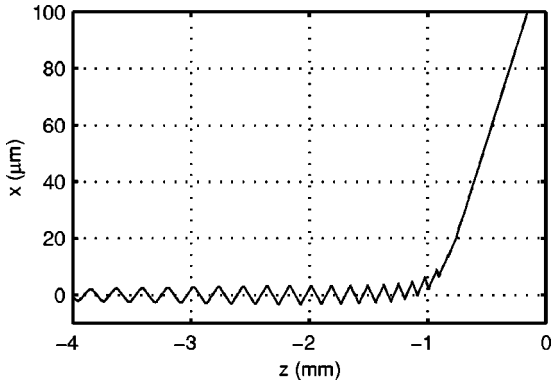

FIG. 13. Two-dimensional electron trajectory in the x-z plane computed using the exact fields, with the same parameters as in Fig. 11.

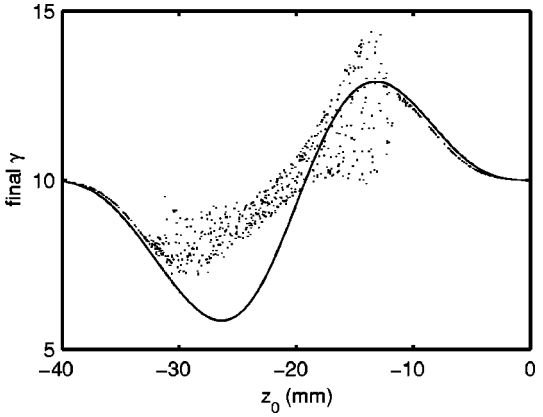

FIG. 14. Final electron Lorentz factor as a function of its initial position along the laser propagation axis. The trajectory is computed using the exact fields (dots) and the RPF (solid line). The parameters are $a=5.34$, $w_0=4.95\ \mu$m, $\Delta\tau=350$ fs, and $\gamma_0=10$.

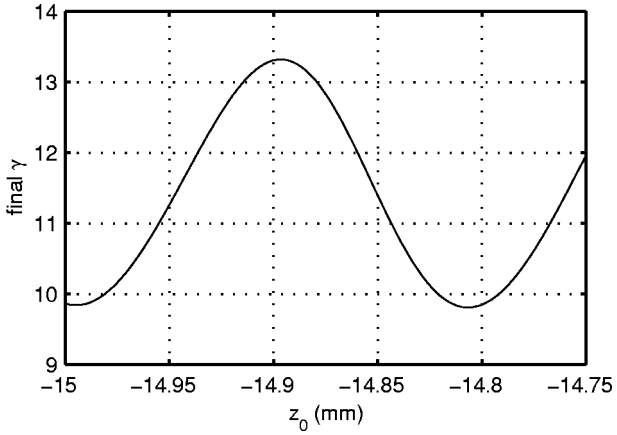

FIG. 15. Final electron Lorentz factor as a function of its initial position along the laser propagation axis for the same parameters as Fig. 14, except $x_0=10^{-2}\ \mu$m, and $y_0=0$. Method (4) (exact fields) is used here.

of the behavior of the electron lies in the complex structure of the electromagnetic field around the focus more than in the high value of the electron excursion around its mean position. This dramatic modification of the electron motion due to the inclusion of the longitudinal fields can be understood if we consider the fields in the initial rest frame of the electron, that is the frame moving at speed $v_0\mathbf{e}_z$ with respect to the laboratory frame. If we note with a prime the quantities in this moving frame, then $|\mathbf{E}_z'|=|\mathbf{E}_z|$ and $|\mathbf{E}_x'|=\gamma_0(1-v_0/c)|\mathbf{E}_x|$: the longitudinal fields are unaffected, but the transverse field is reduced by the factor $\gamma_0(1-v_0/c)\simeq 1/2\gamma_0$. Consequently, $|\mathbf{E}_z'|=\epsilon|\mathbf{E}_x|$ and $|\mathbf{E}_x'|=(1/2\gamma_0)|\mathbf{E}_x|$. The numerical values are $\epsilon\simeq 1/120$ and $1/2\gamma_0=1/20$, so that the longitudinal and transverse fields are about of the same order in the initial rest frame of the electron.

The importance of the correct description of the fields is also visible on the study of the final electron energy as a function of its initial longitudinal position on the laser axis before focus. We take as parameters $a=5.34$, $w_0=4.95\ \mu$m, $\Delta\tau=350$ fs, and $\gamma_0=10$. These differ from the parameters of Fig. 15 of Ref. [9] only in the fact that $\Delta\tau=350$ fs instead of 800 fs. We made this change because it shortens the simulation time, which otherwise would have made this study almost impossible on our computing machines. We checked that the results with the first order fields were not affected in their main features by this change. This certainly implies that the results obtained with the exact fields [method (4)] will also be very similar.

Figure 14 shows the final electron γ factor as a function of its initial position on the z axis for 783 points randomly chosen in the interval. The dots correspond to the trajectories computed with the exact fields [method (4)], while the solid curve is the result of the RPF [method (1)]. As for Fig. 4 in the nonrelativistic regime, the effect of the longitudinal ponderomotive force is clearly visible, but the effect of the high initial velocity of the electron is to add a kind of dispersion around a ''mean curve'' which would be very close to the relativistic ponderomotive curve. Another interesting feature of this curve is the fact that it has a pseudoperiod of $\tilde{\lambda}\simeq 200\ \mu$m, as can be seen in Fig. 15, which is a zoom between $z_0=-15$ and -14.75 mm, with $x_0=10^{-2}\ \mu$m and $y_0=0$. This pseudoperiod in z can be explained as follows: in the initial rest frame of the electron, $\tilde{\lambda}$ transforms to $\tilde{\lambda}'=\tilde{\lambda}/\gamma_0\simeq 20\ \mu$m, while the Doppler effect causes the laser wavelength to be precisely $\lambda_0'=\lambda_0/[\gamma_0(1-v_0/c)]\simeq 20\lambda_0=20\ \mu$m in this frame. Therefore, if the initial position of the electron is changed by $\tilde{\lambda}$ in the laboratory frame, it will see the electromagnetic field of the pulse with the same phase relative to the envelope, which explains that both trajectories will be very similar.

As in the previous case, we also simulated a ''beam'' of 1000 electrons with an initial position randomly chosen using a Gaussian distribution. Here $r_0=1\ \mu$m and $z_0=-15$ mm, with $\gamma_0=10$ as above. We can see in Table I that the RPF is no longer valid in this regime of parameters, as Figs. 13 and 14 suggested. This does not mean, however, that the electron motion is purely 2D, as can be seen in Fig. 16 which represents the final $\mathbf{p}_\perp$ of the electrons. Clearly, the electrons with a nonzero y_0 have a final momentum with a nonzero p_y component. The escape angle of the electron is plotted in Fig. 17 (circles), and we can see that it is very different from the theoretical value of formula (50) (solid

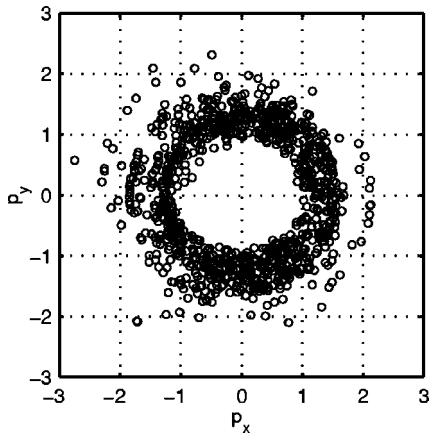

FIG. 16. Final transverse momentum of the electrons for the parameters of Fig. 14 and with $z_0=-15$ mm. The 1000 electrons are initially distributed randomly using a Gaussian probability, with $r_0=1\ \mu$m (see text). The trajectories are computed with the exact fields.

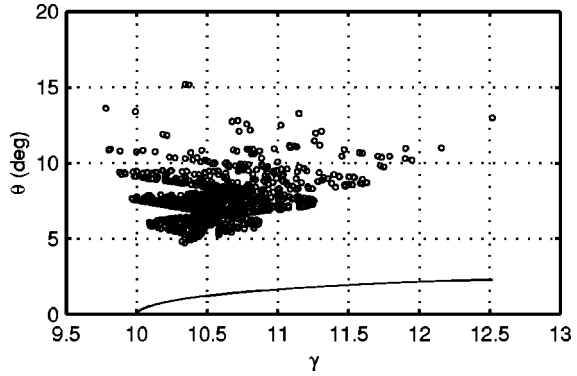

FIG. 17. Ejection angle of the electrons vs their final Lorentz factor. The initial conditions are as in Fig. 16. The open circles correspond to the trajectories computed using the exact fields [method (4)], while the solid line corresponds to theoretical formula (50).

line). The ''oscillations'' that are visible on this figure can be understood by looking at the two following figures (18 and 19) which show the three final components of **p** for electrons initially on the x and y axes, with the other parameters as in the previous figure. When initially along the x axis (that is in the plane of polarization), the electrons gain no momentum in the y direction, as expected [see Fig. 18(b)]. On the other hand, the electrons initially in the y-z plane gain a small p_x when their initial position approaches the laser propagation axis [see Fig. 19(a)]. Note also that p_x in this case has the same oscillating shape as p_x and p_z in Figs. 18(a) and 18(c). This increasing sensitivity to the initial position as the electron approaches the laser axis is the consequence of the high value of the quiver amplitude in this case, which prevents the usual development around the oscillation center motion to be valid. Note on the opposite that the curve $p_y(y_0)$ [Fig. 19(b)] is very like in the RPF case. This comes from the fact that the scattering is due here to the B_z field, as seen before, so that the high oscillating amplitude has only a small effect.

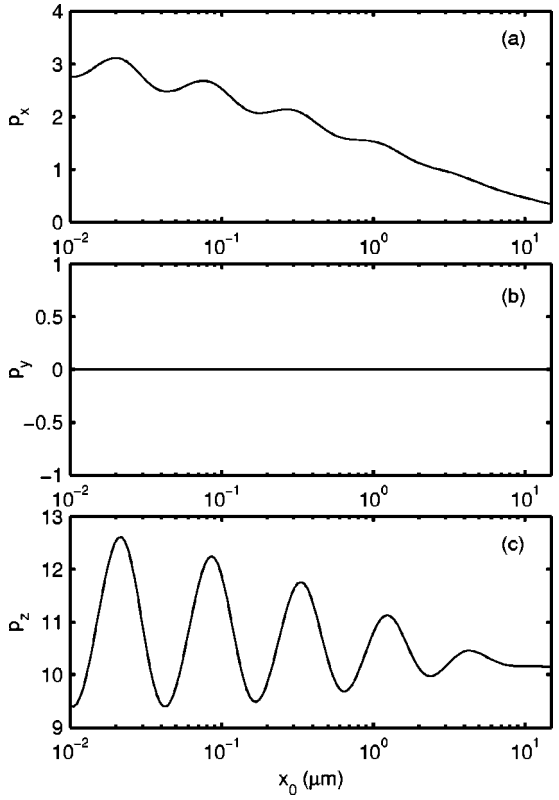

FIG. 18. Components of the final momentum as a function of the initial electron position along the x axis. The parameters are as in Fig. 16.

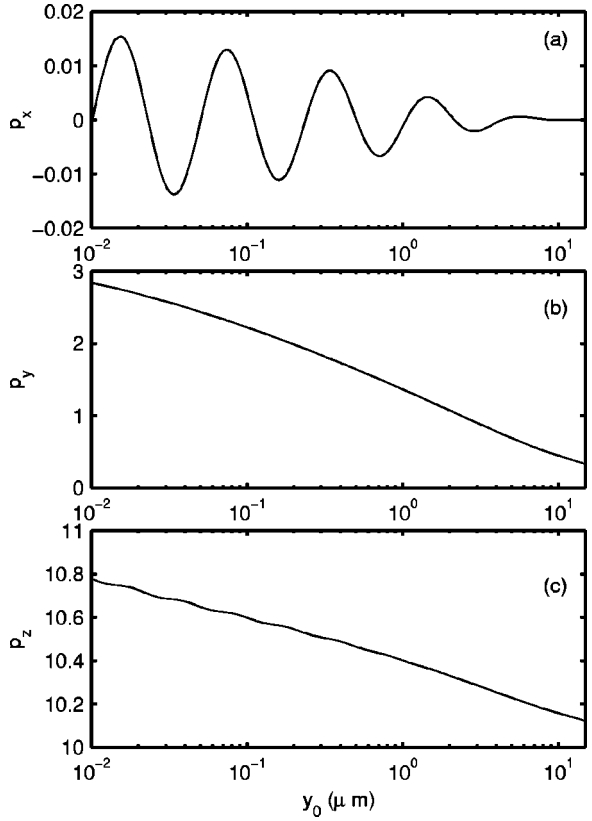

FIG. 19. Components of the final momentum as a function of the initial electron position along the y axis. The parameters are as in Fig. 16.

V. CONCLUSION

In this paper, we have studied theoretically and numerically the motion of electrons in the field of a high intensity laser near focus. A precise demonstration of the relativistic ponderomotive force has been given which makes apparent its limit of validity. This demonstration is based on a complete description of the electromagnetic field of a laser near focus. We have given exact expressions of the fields for the case of a Gaussian profile. These expressions contain as limiting cases the usual zero (paraxial) and first order expressions in the small parameter $\epsilon = 1/kw_0$. We have also derived the first-order corrections which arise when very short pulses are considered, in which case the small parameter is $\sigma = \lambda_0/c\Delta\tau$.

We have performed 3D computer simulations using a test-particle computer code. For the pulses we studied, we have shown that first order corrections in σ were not needed, so that our code gives the *exact* electron motion when we use it with the fields correct to all orders in ϵ. This has allowed us to give the condition of validity of the RPF, which reads $1 - v_z/c \gg \epsilon$: this is valid even at very high laser intensities,

provided that the initial electron velocity in the direction of propagation of the pulse is not too high. The electron is then scattered in the direction of the intensity gradient, with energies of the order of several MeV in the case of very high-intensity pulses. A precise relation exists between its escape angle and its energy, which is, however, slightly different from the one which is usually assumed [Eq. (50)]. This correction to this relation is of great interest in the context of future experiments. A need of such experiments appears as the only previous one [10] is clearly in disagreement with the above results. We have shown, however, that the 2D theoretical model on which this experiment is based is insufficient.

In the regime where the RPF is no longer valid ($1 - v_z/c \lesssim \epsilon$), the electron motion is much more complicated. First, the net energy gain is considerably lower than previously predicted [9], due to the importance of the longitudinal fields in the Lorentz transformed frame where the electron is initially at rest. Second, no definite relation exists between the electron escape angle and its energy in this regime. Third, a high dependence of the electron trajectory on its initial distance from the laser propagation axis appears. This effect is greatest when the electron is in the plane of polarization, but also persists out of this plane. Although it reaches high values, the electron quiver amplitude remains lower than the beam waist, so that the electron motion is 3D, and a 2D code is insufficient.

It is therefore very unlikely that a single laser pulse be a good method to accelerate beams of electrons to very high energies in vacuum. Other, more sophisticated, schemes will probably have better results in this context [29,30].

Finally, we note that special laser field configurations can lead to a (quasi) 2D motion. This can be the case, for instance, if cylindrical lenses are used, or if the focal spot is highly elliptical. Computations in this last case are currently in progress, and will be the object of a future publication.

ACKNOWLEDGMENTS

The authors wish to acknowledge interesting discussions with Tom Antonsen, Jr. and Erik Lefebvre.

[1] G. Mourou and D. Umstadter, Phys. Fluids B **4**, 2315 (1992).
[2] T. W. B. Kibble, Phys. Rev. **150**, 1060 (1966).
[3] W. L. Kruer, *The Physics of Laser Plasma Interactions* (Addison-Wesley, New York, 1988).
[4] G. Schmidt and T. Wilcox, Phys. Rev. Lett. **31**, 1380 (1973).
[5] D. Bauer, P. Mulser, and W.-H. Steeb, Phys. Rev. Lett. **75**, 4622 (1995).
[6] P. Mora and T. M. Antonsen, Jr., Phys. Rev. E **53**, R2 068 (1996).
[7] P. Mora and T. M. Antonsen, Jr., Phys. Plasmas **4**, 217 (1997).
[8] E. A. Startsev and C. J. McKinstrie, Phys. Rev. E **55**, 7527 (1997).
[9] F. V. Hartemann *et al.*, Phys. Rev. E **51**, 4833 (1995).
[10] G. Malka, E. Lefebvre, and J.-L. Miquel, Phys. Rev. Lett. **78**, 3314 (1997).
[11] P. Mora and B. Quesnel, Phys. Rev. Lett. **80**, 1351 (1998).
[12] K. T. McDonald, Phys. Rev. Lett. **80**, 1350 (1998); E. Lefebvre, G. Malka, and J.-L. Miquel, *ibid.* **80**, 1352 (1998).
[13] H. Kogelnik and T. Li, Proc. IEEE **54**, 1312 (1966).
[14] M. Lax, W. H. Louisell, and W. B. McKnight, Phys. Rev. A **11**, 1365 (1975).
[15] L. W. Davis, Phys. Rev. A **19**, 1177 (1979).
[16] G. P. Agrawal and D. N. Pattanayak, J. Opt. Soc. Am. **69**, 575 (1979).
[17] J. P. Barton and D. R. Alexander, J. Appl. Phys. **66**, 2800 (1989).
[18] L. Cicchitelli, H. Hora, and R. Postle, Phys. Rev. A **41**, 3727 (1990).
[19] P. C. Clemmow, *The Plane Wave Spectrum Representation of Electromagnetic Fields* (Pergamon, Oxford, 1966), pp. 22–38.
[20] J. W. Goodman, *Introduction to Fourier Optics* (McGraw Hill, New York, 1968), pp. 48–56.
[21] W. H. Carter, J. Opt. Soc. Am. **62**, 1195 (1972).
[22] B. Rau, T. Tajima, and H. Hojo, Phys. Rev. Lett. **78**, 3310 (1997).
[23] W. Press, S. Teukolsky, W. Vetterling, and B. Flannery, *Numerical Recipes* (Cambridge University Press, Cambridge, 1992), Chap. 16, pp. 708–716.
[24] B. W. Boreham and H. Hora, Phys. Rev. Lett. **42**, 776 (1979).
[25] B. W. Boreham and B. Luther-Davies, J. Appl. Phys. **50**, 2533 (1979).
[26] P. H. Bucksbaum, M. Bashkansky, and T. J. McIlrath, Phys. Rev. Lett. **58**, 349 (1987).
[27] P. Monot *et al.*, Phys. Rev. Lett. **70**, 1232 (1993).
[28] C. I. Moore, J. P. Knauer, and D. D. Meyerhofer, Phys. Rev. Lett. **74**, 2439 (1995).
[29] P. Sprangle, E. Esarey, and J. Krall, Phys. Plasmas **3**, 2183 (1996).
[30] B. Hafizi *et al.*, Phys. Rev. E **55**, 5924 (1997).